Composites Science and Technology 136 (2016) 53–60

Contents lists available at ScienceDirect

Composites Science and Technology

journal homepage: http://www.elsevier.com/locate/compscitech

Reinforcing properties of bacterial polyester with different cellulose nanocrystals via modulating hydrogen bonds

Hou-Yong Yu [a, b, **], Ju-Ming Yao [a, b, *]

[a] The Key Laboratory of Advanced Textile Materials and Manufacturing Technology of Ministry of Education, College of Materials and Textile, Zhejiang Sci-Tech University, Hangzhou 310018, China
[b] National Engineering Lab for Textile Fiber Materials & Processing Technology, Zhejiang Sci-Tech University, Hangzhou 310018, China

ARTICLE INFO

Article history:
Received 7 January 2016
Received in revised form
31 July 2016
Accepted 5 October 2016
Available online 6 October 2016

Keywords:
Nano composites
Interface
Thermal properties
Infrared (IR) spectroscopy

ABSTRACT

This work provides a direct evidence to investigate relationship between hydrogen bonding interactions and property enhancement of cellulose nanocrystals (CN) based bionanocomposites. Cellulose nanocrystal citrates (CN–C) with more hydroxyl (O–H) and carboxyl groups, CN and cellulose nanocrystal formates (CN–F) with less O–H groups were extracted from commercial microcrystalline cellulose using citric/hydrochloric acids, hydrochloric acid and formic/hydrochloric acids, respectively. Then different nanocrystals were incorporated into bacterial polyester poly(3-hydroxybutyrate-co-3-hydroxyvalerate) (PHBV) for tuning hydrogen bonding interactions and properties of PHBV nanocomposites. As expected, at the same loading contents, CN–C had stronger reinforcing capability on PHBV matrix than CN and CN–F. Compared to neat PHBV, tensile strengths of 10% CN–F/PHBV, 10% CN/PHBV and 10% CN–C/PHBV were improved by 146%, 166% and 187%, respectively. Especially, the maximum decomposition temperature of 10% CN–C/PHBV was increased by 48.1 °C, and this nanocomposite showed superior barrier properties with a 64% reduction in water vapour permeability (WVP). Besides, the nanocomposites showed excellent biocompatibility to human MG-63 cells and lower overall migration levels. Such an outstanding reinforcement by CN–C was ascribed to improved interfacial interaction (more hydrogen bonding interactions or hydrogen bond network), and nanodispersibility in the nanocomposites.

1. Introduction

It is well known that uses of conventional non-biodegradable materials (especially food packaging) will cause harmful effects on environment, thus there is a growing interest in developing fully biodegradable polymer based nanocomposites (as biopackagings), especially cellulose nanoparticles (CNPs)-reinforced nanocomposites. With only a small amount of nanofiller addition, mechanical or/and thermal properties of polymer matrix are improved substantially [1–5]. For fully biodegradable nanocomposites, researchers believe that the outstanding and effective polymer reinforcement by CNPs is mainly attributed to strong intermolecular hydrogen bonds between O–H groups of CNPs and C=O groups of biodegradable polyester [poly(3–hydroxybutyrate–co–3–hydroxyvalerate) (PHBV) [6–12], polylactic acid (PLA) [13–15], polycaprolactone (PCL) [16–18]. Many studies have reported that good dispersion of CNPs in polymer matrix was beneficial to form more hydrogen bonding interactions between them, but relationship between surface functional groups of CNPs and hydrogen bonding interactions in nanocomposites was not clear.

Recently, many attempts have been made to explain the reinforcing effect of CNPs on PHBV matrix. Ten et al. found that formation of more hydrogen bonding interactions and nucleating effect of CNPs on PHBV were responsible for significant improvement in mechanical property [10–12]. They found that solution-cast nanocomposites showed better mechanical properties than those of melt-processed nanocomposites due to severe CNP agglomeration. Although polyethylene glycol as a compatibilizer can improve the CNPs dispersion in PHBV matrix, it would restrict the formation of hydrogen bonding interactions between nanofillers and matrix, resulting to a reduction of thermal stability [10,11]. Our study on this nanocomposite system also indicated that

* Corresponding author. The Key Laboratory of Advanced Textile Materials and Manufacturing Technology of Ministry of Education, College of Materials and Textile, Zhejiang Sci-Tech University, Hangzhou 310018, China.
** Corresponding author. The Key Laboratory of Advanced Textile Materials and Manufacturing Technology of Ministry of Education, College of Materials and Textile, Zhejiang Sci-Tech University, Hangzhou 310018, China.
E-mail addresses: phdyu@zstu.edu.cn (H.-Y. Yu), yaoj@zstu.edu.cn (J.-M. Yao).

http://dx.doi.org/10.1016/j.compscitech.2016.10.004
0266-3538/

at the same loading levels, the well-dispersed cellulose nanocrystals (CN) with sulfate groups (CN–S) show weaker reinforcing effects on PHBV than that of HCl-hydrolyzed CN (CN–H). By introduction 10 wt % CN–S or CN–H, tensile strength for 10% CN–S/PHBV was improved by 149% while, the tensile strength for 10% CN–H/PHBV was increased greatly by 166% [8]. The improvement in CN–H/PHBV might be attributed to more hydroxyl groups (without substituted sulfate groups) for forming more hydrogen bonds (supported by larger hydrogen bond fraction value of 0.41 than 0.47 for 10% CN–S/PHBV) [8]. When PHBV chains were grafting on the CNs to improve their dispersion within PHBV matrix, but a decrease in increment magnitude of mechanical properties for the nanocomposite was found as compared to PHBV nanocomposites reinforced by unmodified CNs, which was attributed to decreased amounts of hydroxyl groups and resultant hydrogen bonds [6]. Besides, the graft polymerization of CN needs more complicated processes.

It has been known that enhancements in the mechanical and thermal performances of biopolymer based nanocomposites can be tailored by interactions between CN functional groups and biopolymer groups. Especially, the more hydroxyl groups of CNs have, the more hydrogen bonds between nanofillers and matrix form [5–18]. Nevertheless, to the best of our knowledge, structural design of cellulose nanocrystals for modulating the formation of hydrogen bonds in nanocomposites is still poorly investigated. Therefore, the aim of this work is to endow CNs with different number of hydroxyl groups via HCOOH/HCl and $C_6H_8O_7$/HCl hydrolysis of commercial microcrystalline cellulose (MCC) according to previously described method in our literature [19–21]. In order to evaluate the impact of hydrogen bonding interactions on properties of PHBV nanocomposites, CN samples with different amounts of hydroxyl groups were prepared. Bionanocomposites composed of unmodified CN, cellulose nanocrystal formates (CN–F) and cellulose nanocrystal citrates (CN–C), in a PHBV matrix were produced via simple solution casting. The microscopic structure as well as mechanical, thermal, barrier and migration properties of the nanocomposites were systematically investigated to elucidate the relationship between hydrogen bonding interactions and macroscopic performance reinforcements and thus shed some light on a fast ongoing field of high-performance food biopackagings.

2. Experimental section

2.1. Materials, preparation of CNPs and their nanocomposites

Poly(3-hydroxybutyrate-co-3-hydroxyvalerate) (PHBV, $M_n = 5.90 \times 10^4$) was purchased from Tiannan Biological Material Co., Ltd. Commercial microcrystalline cellulose (MCCs), hydrochloric acid (HCl), acetone and chloroform were purchased from Shanghai Guoyao Group Chemical Reagent Co., Ltd. Citric acid ($C_6H_8O_7$), formic acid (HCOOH) and ammonia solution ($NH_3 \cdot H_2O$) were purchased from Hangzhou Gaojing Fine Chemical Industry Co., Ltd. The preparation and characterization for cellulose nanocrystals (CN), cellulose nanocrystal formates (CN–F), cellulose nanocrystal citrates (CN–C) and the resulting nanocomposites (using solvent casting) were given in Supplementary Information.

3. Results and discussions

The morphology and dispersion of CN, CN–F and CN–C in water were observed by using TEM (Fig. 1). After water evaporation, individual nanocrystals can still be clearly distinguished. The average geometric characteristics of CNs were estimated at 265 ± 30 nm in length and 16 ± 4 nm in diameter. It was in accordance with nanocrystal dimensions reported by published work [21]. For CN–F and CN–C, rod-shaped structure kept and similar dimension achieved. The average aspect ratios (AR) for CN, CN–F and CN–C were about 16.5 ± 7.5, 16.4 ± 8.8 and 16.6 ± 8.4, respectively. The rod-like morphology and geometric dimensions were similar to data reported for CNs extracted from MCC [10,11].

Generally, a homogenous nanocrystal dispersion is prerequisite for forming more intermolecular hydrogen bonds in nanocomposites, thus fractured surfaces of nanocomposite films are studied by FE-SEM. In Fig. 1 and 10% CNs, 10% CN–F and 10% CN–C without micro-scale agglomerates were homogenously dispersed into PHBV matrix, demonstrating that solvent-exchange approach can prevent aggregation of nanocrystals [6–8]. Also, surface groups (formate [9] and citrate groups) contributed to improve uniform distribution of nanocrystals within PHBV matrix. Indeed, a good nanocrystal dispersion in nanocomposites was beneficial to enhance interfacial adhesion between two components and effective stress transfer during mechanical tensile test.

FT-IR analysis is used to confirm different surface functional groups on the CN, CN–F and CN–C. Compared with those of CNs, new strong peaks at 1720 and 1718 cm^{-1} assigning to ester C=O stretching vibrations were observed in spectra of CN–F and CN–C (Fig. 2a), indicating that formate and citrate groups were introduced onto the nanocrystals, respectively. By using oxime reaction and conductivity titration (Supplementary Information), the contents for CN–F formate groups and CN–C carboxyl groups were 0.58 and 1.12 mmol/g, respectively. On the other hand, hydrogen bonding interactions between CNPs and PHBV matrix were confirmed by IR spectra. Peak at 3436 cm^{-1} was due to free O–H groups, while peak at 3345 cm^{-1} was due to hydrogen bonded O–H groups. Moreover, compared with neat PHBV, the band position for C=O stretching was shifted from 1723 to 1727 cm^{-1} and this band became broad for the nanocomposites. These results proved the formation of hydrogen bonding interactions between O–H groups of CNPs and C=O groups of PHBV. Further, hydrogen bond fraction (F_{H-CO}) was calculated through curve–fitting procedure according to reported equation [11,19]:

$$F_{H-CO} = \frac{A_H \Big/ r_{H/a}}{\left(A_H \Big/ r_{H/a} + A_a\right)}, \quad (1)$$

where A_a and A_H are peak areas of free and hydrogen bonded components, respectively, and $r_{H/a}$ is the specific absorption ratio of above two bands.

Fig. 2b illustrates that at the same loading levels, F_{H-CO} value of CN–C based nanocomposite was larger than that of CN based nanocomposite, whereas the CN–F based nanocomposite showed lowest F_{H-CO} values. It indicates the formation of more intermolecular hydrogen bonds in the CN–C based nanocomposites due to more polar groups (carboxyl and hydroxyl groups) on CN–C (Fig. 2c) with good dispersion in matrix (Fig. 1). Indeed, the hydrogen bonds took place by hydroxyl or carboxyl groups (CNPs) as proton donors and carbonyl groups (PHBV) as proton acceptors. The CN–C had more hydroxyl or carboxyl groups after one hydroxyl group of cellulose was esterified with carboxyl group of $C_6H_8O_7$, leading to two carboxyl and one hydroxyl groups on each cellulose unit(Fig. 2d). Therefore, larger amounts of hydrogen bonds were obtained for the CN–C based nanocomposites. On the contrary, hydroxyl groups of CN–F were reacted with carboxyl groups of HCOOH, and thus the amounts of hydroxyl groups were reduced, leading to a decrease in numbers of hydrogen bonds.

CNPs can simultaneously form two intermolecular hydrogen bonds with PHBV due to two C=O groups in each unit of PHBV [6–8,22], which was defined as double hydrogen bonded CNPs (db-

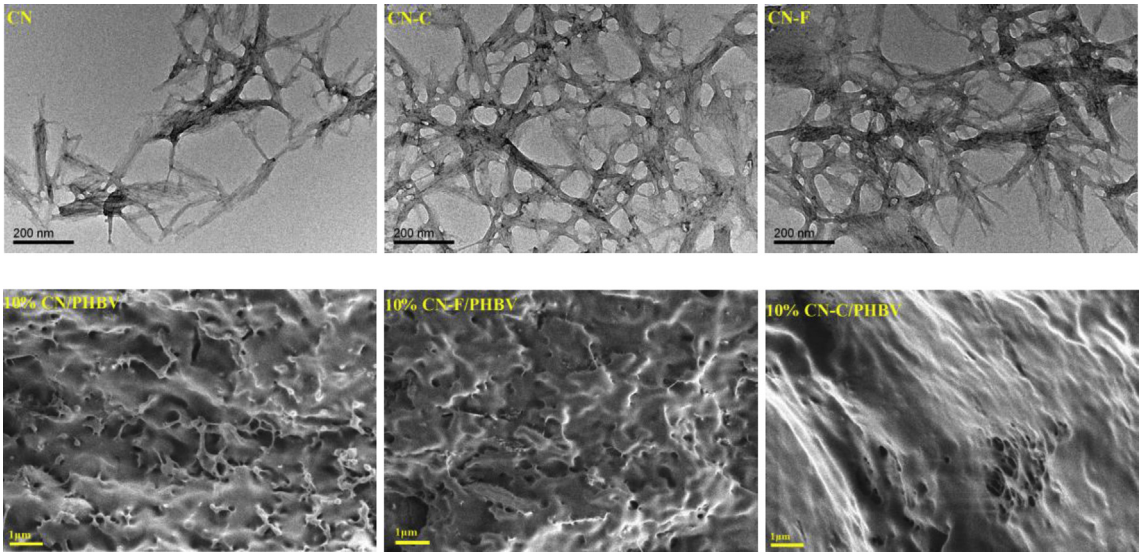

Fig. 1. TEM micrographs of CN, CN–F and CN–C; and FE-SEM images for fractured morphologies of 10% CN/PHBV, 10% CN–F/PHBV and 10% CN–C/PHBV.

CNPs). In general, the number of O–H groups (N_{H-OH}) involved in hydrogen bonds should be equal to that of hydrogen bonded C=O groups (N_{H-CO}), the fraction of hydroxyl groups involved in intermolecular hydrogen bonds (F_{H-OH}) and fraction of db-CNPs ($F_{db-CNPs}$) can be calculated as follows:

$$N_{H-OH} = N_{H-CO}, \tag{2}$$

$$F_{H-OH} = F_{H-CO}(1 - X_c)\Big/R_{OH/CO}, \tag{3}$$

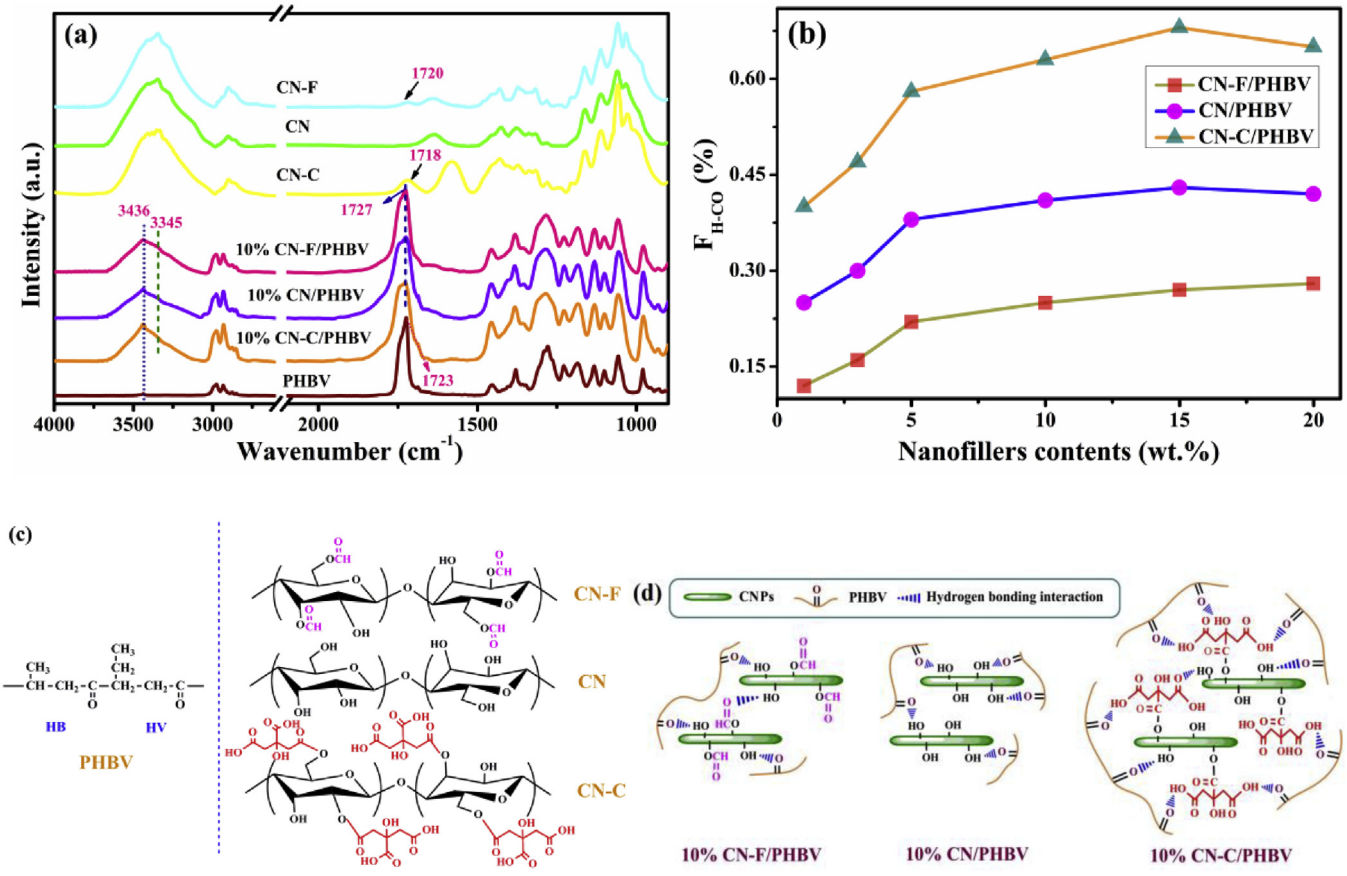

Fig. 2. FT-IR spectra (a), hydrogen bond fraction (F_{H-CO}) (b), chemical structures (c) for PHBV and different nanocrystals (CN, CN–F and CN–C) and the nanocomposites, (d) schematic representation for possible formation of hydrogen bonding interactions in 10% CN/PHBV, 10% CN–F/PHBV and 10% CN–C/PHBV.

$$F_{db-CNPs} \geq 2F_{H-OH} - 1, \quad (4)$$

Where X_c is crystallinity of nanocomposites, $R_{OH/CO}$ is the molar ratio of O–H groups and C=O groups in nanocomposites, and can be calculated by following equations:

$$(\text{CN/PHBV nanocomposite}): R_{OH/CO} = \frac{\frac{m_{CNPs}}{M_{CNPs}} \times 3}{\frac{m_{PHBV}}{M_{PHBV}} \times 2}, \quad (5)$$

$$(\text{CN} - \text{F/PHBV nanocomposite}): R_{OH/CO} = \frac{\frac{m_{CNPs}}{M_{CNPs}} \times 3 - n_{OCOH} \times m_{CNPs}}{\frac{m_{PHBV}}{M_{PHBV}} \times 2}, \quad (6)$$

$$(\text{CN} - \text{C/PHBV nanocomposite}): R_{OH/CO} = \frac{\frac{m_{CNPs}}{M_{CNPs}} \times 3 + n_{COOH} \times m_{CNPs}}{\frac{m_{PHBV}}{M_{PHBV}} \times 2}, \quad (7)$$

where m_{CNPs} and m_{PHBV} are weights of CNPs and PHBV, respectively; M_{CNPs} (162 g mol^{-1}) and M_{PHBV} (154 g mol^{-1}) are molecular weigh for repeating units of cellulose and PHBV, respectively; n_{OCOH} and n_{COOH} are formate and carboxyl contents, respectively.

As shown in Table 1, $F_{db\text{-}CNPs}$ value of 10% CN–F/PHBV was about 0.30, indicating that more than 30% of CN–F nanofillers formed two hydrogen bonds with PHBV chains. This strongly hints that there is a hydrogen-bonding network in the nanocomposites. Moreover, higher $F_{db\text{-}CNPs}$ of 1.46 and 2.66 were found for 10% CN/PHBV and 10% CN–C/PHBV, respectively. It suggests that denser hydrogen-bonding network was formed in 10% CN–C/PHBV nanocomposites, which were supported by percolation threshold (PT) value of CN–C nanoparticles. Based on aspect ratios (AR) of CNPs and equation of percolation threshold (PT = 0.7/AR) [11,23,24]. Therefore, the percolation threshold of CNPs was calculated to be 4.2 vol % using the CNP aspect ratio of 16.5. With known densities of PHBV (1.2 g/cm^3) and CNPs (1.5 g/cm^3) [11,25], the percolation threshold in CNP weight ratio was 5.2 wt %. Above this weight ratio of CNPs, the continuous percolation network was easily obtained due to homogeneous dispersion of CNPs and strong hydrogen bonding interactions between PHBV and CNPs. Generally, the hydrogen bond forms a physical crosslink in the nanocomposites and exerts a great influence on the nanocomposite properties [11,22].

From Eqs. (4)–(7), the fraction of C=O group that acts as a crosslink point ($F_{L\text{-}CO}$) and average number of atoms between every two adjacent crosslink points ($N_{L\text{-}L}$) can be determined as follows:

$$F_{L-CO} = F_{db-CNPs} R_{OH/CO} \Big/ (1 - X_c), \quad (8)$$

$$N_{L-L} = 4/F_{L-CO}, \quad (9)$$

The calculated values of $F_{L\text{-}CO}$ and $N_{L\text{-}L}$ are listed in Table 1. Clearly, 10% CN–C/PHBV showed the largest $F_{L\text{-}CO}$ value (0.92) than those of other nanocomposites, indicating the highest crosslink density for 10% CN–C/PHBV, whereas the $N_{L\text{-}L}$ was less than 4.36. It has been reported that high density hydrogen-bonding network of PHBV/bisphenol a nanocomposites would suppress the PHBV crystallization. This confined crystal structure may bring a beneficial effect on PHBV morphology, and improved mechanical properties [12,22].

Table 1
Estimated parameters based on F_{H-CO} values for the nanocomposites reinforced with different CNPs.

Sample	F_{H-CO}	$R_{OH/CO}$	F_{H-OH}	$F_{db\text{-}CNPs} \geq$	$F_{L\text{-}CO} \geq$	$N_{L\text{-}L} \leq$
10%CN/PHBV	0.41	0.16	1.23	1.46	0.49	8.22
10%CN–F/PHBV	0.25	0.15	0.65	0.30	0.12	34.39
10%CN–C/PHBV	0.63	0.17	1.83	2.66	0.92	4.37

Fig. 3a and b illustrate DSC curves, T_c and $T_{c\ (onset)}$-T_c of neat PHBV and the nanocomposites reinforced with different CNPs, and the corresponding thermal parameters (crystallization temperature (T_c), cold crystallization temperature (T_{cc}), and onset temperature of crystallization ($T_{c\ (onset)}$)) are listed in Table 2. No obvious crystallization peak appeared in the first cooling scans of neat PHBV, and only cold crystallization peak (41.2 °C) was observed in the second heating scan (Fig. 3a), while strong crystallization peaks at 54.1, 100.4 and 78.0 °C were found for 10% CN–F/PHBV, 10%CN/PHBV and 10%CN–C/PHBV, respectively. These results implied easier crystallization of PHBV occurred in the presence of the CNPs, and the heterogeneous nucleation effect of CNs was stronger than other nanofillers. The 10%CN/PHBV had higher T_c and lower $T_{c\ (onset)}$-T_c values than those of PHBV and other nanocomposites (Fig. 3b and Table 2), revealing that the incorporation of CNs could efficiently induce a greater increase in nucleation and crystallization rates of PHBV crystals because the parameter $T_{c\ (onset)}$-T_c is used to evaluate the overall crystallization rate of the nanocomposites, the smaller $T_{c\ (onset)}$-T_c value hints the greater overall crystallization rate [7,8]. The different T_c values can be explained that only OH groups on CNs could quickly tailor conformational ordering of crystalline PHBV chains, and thus PHBV crystallization could be induced and accelerated by interchain interactions in terms of surface-induced conformational order (SICO), leading to an appearance of higher T_c, as compared to CN–F or CN–C with substituted groups. A similar phenomenon was found for poly (L-lactide) nanocomposites reinforced with carbon nanotubes and graphene nanosheets [26].

The WAXD patterns, crystallinities (X_c) and crystallite size (D_{200}) are shown in Fig. 3c and d. Based on Rietveld-Ruland approach and Scherrer equation, the X_c and D_{200} of the nanocomposites were calculated and listed in Table 2. It has been reported that CNPs can affect the PHBV crystallization in two opposed ways [7,8,12]. On one hand, CNPs was an efficient nucleation agent to promote nucleation and overall crystallization rate, leading to higher crystallization temperature. On the other hand, due to hydrogen bonding interactions, CNPs hindered chain diffusion and folding during PHBV spherulitic growth [8,12], resulting in a slight decrease of crystallinity. In Fig. 3c, the CNPs exhibited characteristic diffractograms of cellulose I, and their incorporation did not cause new crystalline symmetries of PHBV. Furthermore, compared to neat PHBV, the (111) diffraction was shifted to higher angles after CNP addition, suggesting that PHBV formed defective crystals in the presence of CNPs due to hydrogen bonding interaction. As a result, 10% CN–C/PHBV showed the lowest X_c value than other nanocomposites (Fig. 3d) since the diffusion rate of crystalline PHBV chains was altered by hydrogen bond network induced by more hydrogen bonds in the nanocomposite (Table 1). The crystallinity obtained from DSC curves (X_{DSC}) also confirmed the lower X_{DSC} for CN–C/PHBV (Table S1). Meanwhile, all the nanocomposites showed the smaller D_{200} than that of PHBV, implying the confined crystalline PHBV chains with CNPs. It should be noted that 10% CN–F/PHBV displayed the higher X_c value than those of other nanocomposites due to relatively weak hydrogen bonding interactions, which was consistent with FT-IR results (Fig. 2c and Table 1).

Fig. 4a shows the tensile strength, Young's modulus and elongation to break for neat PHBV and nanocomposites reinforced with different CNPs. The addition of CNPs efficiently improved the tensile strength and Young's modulus of PHBV owing to the higher

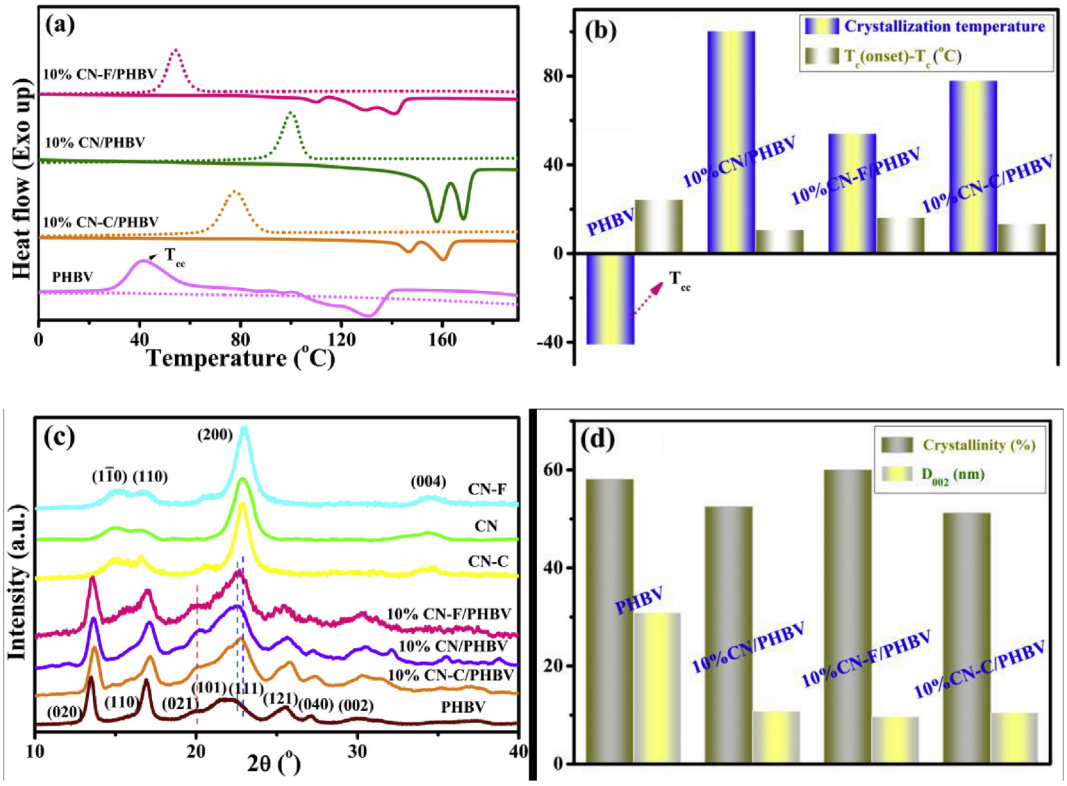

Fig. 3. DSC curves (a), crystallization temperature (T_c) and $T_{c\ (onset)}$-T_c (b), WAXD patterns (c), crystallinity and D_{200} (d) for neat PHBV, different nanocrystals (CN, CN–F and CN–C) and the nanocomposites.

modulus of nanocrystals [1,4,15]. Compared to neat PHBV, the tensile strengths of 10%CN–F/PHBV, 10%CN/PHBV and 10%CN–C/PHBV were improved by 146%, 166% and 187%, respectively. Similar enhancements in Young's modulus were also found. Moreover, 10% CN–C/PHBV showed the higher tensile strength and modulus than others, but lower elongation to break. This greater enhancement was an indication of stronger interfacial bonding/adhesion between CN–Cs and PHBV matrix, which lead to better stress transfer from the soft matrix to the stiff CN–Cs. Since well-dispersed CNPs with similar aspect ratio were introduced to PHBV matrix, hydrogen bonding interactions between two phases were predominant in the nanocomposites. The hydrogen bonding interactions or networks could facilitate efficient load transfer between polymer chains and the percolating network of nanocrystals, endowing additional strength to the nanocomposites [1,11,27]. This explanation was also applied to the change trends of Tensile strength and Young's modulus for nanocomposites containing lower CNP contents (5 wt% CNPs as a model example, Fig. S1). Additionally, the reduction in elongation to break was due to decreased segmental mobility of PHBV chains induced by interactions with CNPs.

Fig. 4b–d shows TGA curves, initial decomposition temperature (T_0), maximum decomposition temperature (T_{max}) and the plot of $\ln[\ln(W_0/W_T)]$ vs. θ for main thermal degradation stage for neat PHBV and the nanocomposites, and main thermal parameters are summarized in Table 2. The T_{max} of CN–C was about 347.4 °C, which was lower than those of CN (363.9 °C) and CN–F (359.4 °C). This result was due to that more thermally unstable carboxyl groups of CN–C would significantly depress the degradation temperature. Generally, the more carboxyl groups were prone to dehydration reaction, so the weight loss in degradation curve of CN–C began at 200 °C (Fig. 4b). Surprisingly, TGA curve of 10% CN–C/PHBV shifted

Table 2
Hydrogen bond fractions (F_{H-CO}), crystallinities and thermal analysis parameters for neat PHBV and the nanocomposites reinforced with different CNPs.

Sample	X_c (%)[a]	D_{200} (nm)[a]	T_c (°C)[b]	$T_{c(onset)}$-T_c (°C)[b]	T_0 (°C)[c]	T_{max} (°C)[c]	T_0-T_{m3} (°C)[d]	E_a (kJ/mol)[e]
PHBV	55.6	30.9	/	24.3	229.4	245.8	99.4	204.0
CN	85.6	6.0	/	/	322.5	363.9	/	186.3
CN–F	86.3	6.0	/	/	338.2	359.4	/	245.6
CN–C	86.5	6.0	/	/	325.3	347.4	/	124.8
10%CN/PHBV	55.3	10.8	100.4	10.7	284.6	293.3	116.0	339.1
10%CN–F/PHBV	57.8	9.7	54.1	16.3	254.9	270.3	113.9	255.6
10%CN–C/PHBV	54.6	10.5	78.0	14.1	286.9	293.9	126.5	482.7

[a] X_c and D_{200} were calculated from WAXD patterns and Scherrer equation, respectively.
[b] Thermal parameters of non–isothermal crystallization was recorded by DSC curves.
[c] The values of T_0 and T_{max} were obtained from TGA curves.
[d] T_0-T_{m3} stood for the melt–processing window.
[e] E_a was calculated by Horowitz and Metzger method.

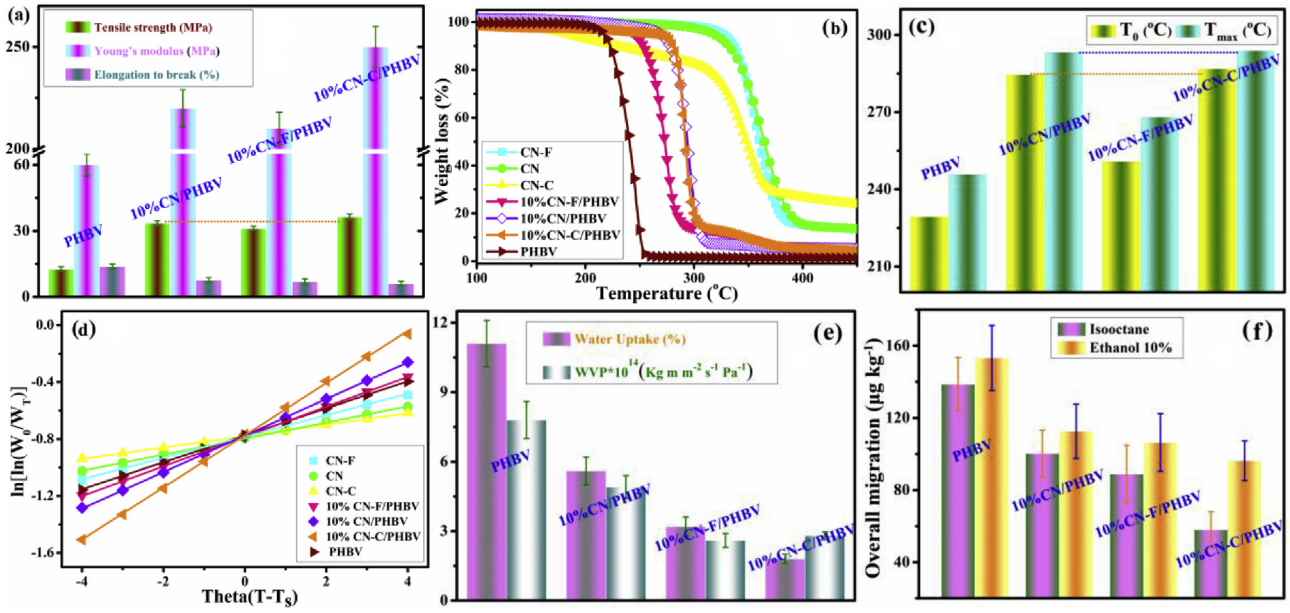

Fig. 4. Tensile strength, Young's modulus, and elongation to break (a), TGA curves (b), T_0 and T_{max} (c), and the plot of ln [ln(W_0/W_T)] vs. θ for main thermal degradation stage (d), water uptake and water vapor permeability (e), overall migration data in ethanol 10% (v/v) and isooctane (f) for neat PHBV and the nanocomposites reinforced with different CNPs.

to higher temperature than those of PHBV and other nanocomposites. The T_0 and T_{max} increased by 57.5 and 48.1 °C, 2.3 and 0.6 °C, 32.0 and 23.6 °C, as compared to neat PHBV, 10% CN/PHBV and 10% CN–F/PHBV (Fig. 4c and Table 2). It indicates that 10% CN–C/PHBV showed the best thermal stability among all the nanocomposites, the reinforcing efficiency of CN–C with the same loading levels on the thermal stability was stronger than CN and CN–F. The reinforcing efficiency was mainly dependent on amounts of intermolecular hydrogen bonds between two components when well-dispersed nanofillers with similar size were employed in the nanocomposite preparation. Larger amounts of hydrogen bonds can restrict the formation of six–membered ring ester during the PHBV degradation process [6–9,28], as a result, the higher thermal stability of PHBV nanocomposites can be achieved by incorporating CN–C.

The results of average apparent activation energy (E_a) calculated from slopes of the fitted lines are given in Fig. 4d and Table 2. Generally, the higher E_a is, the faster degradation rate is [20,28].

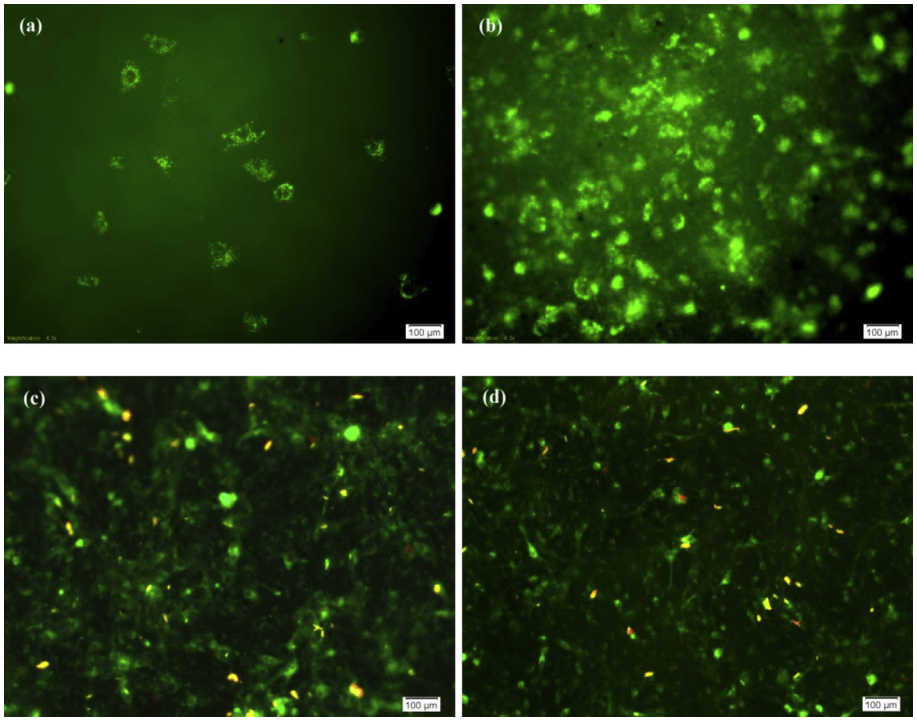

Fig. 5. Fluorescence microscopy images of neat PHBV (a), 10% CN/PHBV (b), 10% CN–F/PHBV (c) and 10% CN–C/PHBV (d).

Table 2 illustrates that E_a value of CN–C was larger than those of CN and CN–F, but 10%CN–C/PHBV had largest E_a value than other nanocomposites, implying that the degradation rate of 10%CN–C/PHBV was quicker than other samples. From above, incorporation of CNPs can influence the degradation behavior of PHBV in two opposite ways. On the one hand, during degradation of PHBV, the addition of CNPs enhanced its thermal stability so that thermal degradation of PHBV begun at a higher temperature, and this higher temperature was a factor to result in an increasing degradation rate of PHBV. On the other hand, the more O–H groups of CNPs would form stronger intermolecular hydrogen bonding interactions with ester C=O groups (10%CN–C/PHBV), which can increase degradation temperature of PHBV matrix.

It is well known that improved interfacial interaction, crystalline structure and crystallinity of the nanocomposites can result in higher tortuosity of transport path and prevent water (vapor) molecules permeating into nanocomposite films [1,9,16,26,29]. The effect of hydrogen bonding interactions on barrier and migration properties of PHBV was investigated. In Fig. 4e and 10%CN–C/PHBV showed the greatest reduction in water uptake and WVP than those of neat PHBV and other nanocomposites, which was ascribed to strong interfacial interaction (hydrogen bonds) between two components. The interactions can slash the number of sorption sites available for moisture sorption in polymer matrix, and reduce the equilibrium moisture content [30]. Compared with neat PHBV, the water uptake and WVP values were reduced by 84% and 64% for 10%CN–C/PHBV, 71% and 67% for 10%CN–F/PHBV, 50% and 37% for 10%CN/PHBV, respectively. It indicates that the nanocomposites exhibited the improved barrier properties against water and water vapor. Similar reduced moisture absorption capability was reported for biopolymer based nanocomposites reinforced with CNPs [22,24]. Moreover, 10%CN–F/PHBV exhibited the larger reduction in water uptake and WVP than that of 10%CN/PHBV, which was due to its relatively higher crystallinity (Table 2).

Results of overall migration levels in Fig. 4f also illustrated that 10% CN–C/PHBV showed lowest migration levels than those of other nanocomposites, which were well below the migration limits (60 mg/kg of simulant) for food contact materials according to Commission Directive, 2002/72/EC [9,19,29]. It indicates that the incorporation of CN–C had the more positive effect on the migration properties of PHBV due to stronger interfacial adhesion or hydrogen bonding network in the nanocompsites. Further, fluorescence microscopy images (Fig. 5) demonstrated that numerous human MG-63 cells (stained green) on the nanocomposite films were observed compared to neat PHBV, indicating that introduction of the CNPs improved biocompatibility and cellular uptake of the nanocomposites. It is found that CNPs with different surface charge/groups can improve efficiently cell-matrix interactions and thus cellular uptake to human embryonic kidney 293 and Spodoptera frugiperda cells [6,31]. It hints that these nanocomposites will be further applied for food contact biopackagings and other biomedical materials.

4. Conclusions

CNPs with different surface groups (CN–F, CN and CN–C) were successfully prepared and used as reinforcement materials for PHBV nanocomposites. It confirms that at good dispersion state of nanofillers, CN–C with more O–H groups could form more intermolecular hydrogen bonds with PHBV matrix. As a result, at the same loading level, greater improvements in the mechanical and thermal properties were found compared to other nanocomposites. Compared with neat PHBV, tensile strengths and T_{max} of 10% CN–C/PHBV were improved by 187% and 48.1 °C, respectively. The nanocomposites showed a 64% reduction in water vapour permeability (WVP) indicating stronger reinforcing capability on PHBV matrix than CN and CN–F. This could be due to stronger interactions (more hydrogen bonds or hydrogen bond network) and their good nanoparticle dispersion. Moreover, overall migration levels of 10%CN–C/PHBV were well below the migration limits for food contact materials and showed excellent biocompatibility to human MG-63 cells. This study provides a method to modulate hydrogen bonding interaction and properties of PHBV nanocomposites, meanwhile the obtained nanocomposites have charming application in food biopackaging materials.

Acknowledgments

The project was funded by the National Natural Science Foundation of China (51403187), the public technology research plan of Zhejiang Province, China under Grant No. 2015C33111, and “521” Talent Project of Zhejiang Sci-Tech University.

Appendix A. Supplementary data

Supplementary data related to this article can be found at http://dx.doi.org/10.1016/j.compscitech.2016.10.004.

References

[1] S. Fujisawa, T. Ikeuchi, M. Takeuchi, T. Saito, A. Isogai, Superior reinforcement effect of TEMPO-Oxidized cellulose nanofibrils in polystyrene matrix: optical, thermal, and mechanical studies, Biomacromolecules 13 (2012) 2188–2194.
[2] M. Pereda, N. El Kissi, A. Dufresne, Extrusion of polysaccharide nanocrystal reinforced polymer nanocomposites through compatibilization with poly(-ethylene oxide), ACS Appl. Mater Interfaces 6 (2014) 9365–9375.
[3] V. Khoshkava, M.R. Kamal, Effect of cellulose nanocrystals (CNC) particle morphology on dispersion and rheological and mechanical properties of PP/CNC nanocomposites, ACS Appl. Mater Interfaces 6 (2014) 8146–8157.
[4] N. Lin, A. Dufresne, Physical and/or chemical compatibilization of extruded cellulose nanocrystal reinforced polystyrene nanocomposites, Macromolecules 46 (2013) 5570–5583.
[5] K. Li, J. Song, M. Xu, S. Kuga, L. Zhang, J. Cai, Extraordinary reinforcement effect of three-dimensionally nanoporous cellulose gels in poly (ε-caprolactone) bionanocomposites, ACS Appl. Mater Interfaces 6 (2014) 7204–7213.
[6] H.Y. Yu, Z.Y. Qin, C.F. Yan, J.M. Yao, Green nanocomposites based on functionalized cellulose nanocrystals: a study on the relationship between interfacial interaction and property Enhancement, ACS Sustain Chem. Eng. 2 (2014) 875–886.
[7] H.Y. Yu, Z.Y. Qin, Y.N. Liu, L. Chen, N. Liu, Z. Zhou, Simultaneous improvement of mechanical properties and thermal stability of bacterial polyester by cellulose nanocrystals, Carbohydr. Polym. 89 (2012) 971–978.
[8] H.Y. Yu, Z.Y. Qin, L. Liu, X.G. Yang, Y. Zhou, J.M. Yao, Comparison of the reinforcing effects for cellulose nanocrystals obtained by sulfuric and hydrochloric acid hydrolysis on the mechanical and thermal properties of bacterial polyester, Compos Sci. Technol. 87 (2013) 22–28.
[9] H. Yu, C. Yan, J. Yao, Fully biodegradable food packaging materials based on functionalized cellulose nanocrystals/poly (3-hydroxybutyrate-co-3-hydroxyvalerate) nanocomposites, RSC Adv. 4 (2014) 59792–59802.
[10] E. Ten, J. Turtle, D. Bahr, L. Jiang, M. Wolcott, Thermal and mechanical properties of poly (3-hydroxybutyrate-co-3-hydroxyvalerate)/cellulose nanowhiskers composites, Polymer 5 (2010) 2652–2660.
[11] E. Ten, D.F. Bahr, B. Li, L. Jiang, M.P. Wolcott, Effects of cellulose nanowhiskers on mechanical, dielectric, and rheological properties of poly (3-hydroxybutyrate-co-3-hydroxyvalerate)/cellulose nanowhisker composites, Ind. Eng. Chem. Res. 51 (2012) 2941–2951.
[12] E. Ten, L. Jiang, M.P. Wolcott, Crystallization kinetics of poly (3-hydroxybutyrate-co-3-hydroxyvalerate)/cellulose nanowhiskers composites, Carbohyd Polym. 90 (2012) 541–550.
[13] A. Pei, Q. Zhou, L.A. Berglund, Functionalized cellulose nanocrystals as biobased nucleation agents in poly (l-lactide) (PLLA)-crystallization and mechanical property effects, Compos Sci. Technol. 70 (2010) 815–821.
[14] A.L. Goffin, Y. Habibi, J.M. Raquez, P. Dubois, Polyester-grafted cellulose nanowhiskers: a new approach for tuning the microstructure of immiscible polyester blends, ACS Appl. Mater Interfaces 4 (2012) 3364–3371.
[15] C. Zhou, Q. Shi, W. Guo, L. Terrell, A.T. Qureshi, D.J. Hayes, Q. Wu, Electrospun bio-nanocomposite scaffolds for bone tissue engineering by cellulose nanocrystals reinforcing maleic anhydride grafted PLA, ACS Appl. Mater Interfaces 5 (2013) 3847–3854.
[16] H. Lonnberg, K. Larsson, T. Lindstrom, A. Hult, E. Malmstrom, Synthesis of polycaprolactone-grafted microfibrillated cellulose for use in novel bionanocomposites-influence of the graft length on the mechanical

properties, ACS Appl. Mater Interfaces 3 (2011) 1426–1433.
[17] Y. Habibi, A. Dufresne, Highly filled bionanocomposites from functionalized polysaccharide nanocrystals, Biomacromolecules 9 (2008) 1974–1980.
[18] J.O. Zoppe, M.S. Peresin, Y. Habibi, R.A. Venditti, O.J. Rojas, Reinforcing poly (ε-caprolactone) nanofibers with cellulose nanocrystals, ACS Appl. Mater Interfaces 1 (2009) 1996–2004.
[19] H. Yu, B. Sun, D. Zhang, G. Chen, X. Yang, J. Yao, Reinforcement of biodegradable poly (3-hydroxybutyrate-co-3-hydroxyvalerate) with cellulose nanocrystal/silver nanohybrids as bifunctional nanofillers, J. Mater Chem. B 2 (2014) 8479–8489.
[20] H.Y. Yu, G.Y. Chen, Y.B. Wang, J.M. Yao, A facile one-pot route for preparing cellulose nanocrystals/zinc oxide nanohybrids with high antibacterial and photocatalytic activity, Cellulose 21 (2014) 1–13.
[21] H.Y. Yu, Z.Y. Qin, B.L. Liang, Liu Na, Z. Zhou, L. Chen, Facile preparation of thermally stable cellulose nanocrystals with high yield of 93 % through hydrochloric acid hydrolysis under hydrothermal condition, J. Mater Chem. A 1 (2013) 3938–3944.
[22] B. Fei, C. Chen, H. Wu, S. Peng, X. Wang, L. Dong, Quantitative FTIR study of PHBV/Bisphenol a blends, Eur. Polym. J. 2003 (1939-1946) 39.
[23] Y. Habibi, L.A. Lucia, O.J. Rojas, Cellulose nanocrystals: chemistry, self-assembly, and applications, Chem. Rev. 110 (2010) 3479–3500.
[24] R. Moon, A. Martini, J. Nairn, J. Simonsen, J. Youngblood, Cellulose nanomaterials review: structure, properties and nanocomposites, Chem. Soc. Rev. 40 (2011) 3941–3994.
[25] W. Gindl, J. Keckes, Tensile properties of cellulose acetate butyrate composites reinforced with bacterial cellulose, Compos Sci. Technol. 64 (2004) 2407–2413.
[26] J.Z. Xu, T. Chen, C.L. Yang, Z.M. Li, Y.M. Mao, B.Q. Zeng, B.S. Hsiao, Isothermal crystallization of poly (l-lactide) induced by graphene nanosheets and carbon nanotubes: a comparative study, Macromolecules 43 (2010) 5000–5008.
[27] J. George, R. Kumar, V.A. Sajeevkumar, K.V. Ramana, R. Rajamanickam, V. Abhishek, S. Nadanasabapathy, Hybrid HPMC nanocomposites containing bacterial cellulose nanocrystals and silver nanoparticles, Carbohyd Polym. 105 (2014) 285–292.
[28] Q.S. Liu, M.F. Zhu, W.H. Wu, Z.Y. Qin, Reducing the formation of six-membered ring ester during thermal degradation of biodegradable PHBV to enhance its thermal stability, Polym. Degrad. Stabil. 94 (2009) 18–24.
[29] A.M. Díez-Pascual, A.L. Diez-Vicente, Zno-reinforced poly (3-hydroxybutyrate-co-3-hydroxyvalerate) bionanocomposites with antimicrobial function for food packaging, ACS Appl. Mater Interfaces 6 (2014) 9822–9834.
[30] E. Espino-Pérez, J. Bras, V. Ducruet, A. Guinault, A. Dufresne, S. Domenek, Influence of chemical surface modification of cellulose nanowhiskers on thermal, mechanical, and barrier properties of poly (Lactide) based bionanocomposites, Eur. Polym. J. 49 (2013) 3144–3154.
[31] K.A. Mahmoud, J.A. Mena, K.B. Male, S. Hrapovic, A. Kamen, J.H. Luong, Effect of surface charge on the cellular uptake and cytotoxicity of fluorescent labeled cellulose nanocrystals, ACS Appl. Mater Inter 2 (2010) 2924–2932.